Quantum-Correlated Photon-Pair Source with Integrated Feedback Control in 45 nm CMOS

D. Kramnik[1†], I. Wang[2], J. M. Fargas Cabanillas[2], A. Ramesh[3], S. Buchbinder[1], P. Zarkos[1], C. Adamopoulos[1], P. Kumar[3], M. A. Popović[2], and V. Stojanović[1‡]
[1]Department of Electrical Engineering and Computer Sciences, UC Berkeley, Berkeley, CA 94720, USA
[2]Department of Electrical and Computer Engineering, Photonics Center, Boston University, Boston, MA 02215, USA
[3]Dept. of Electrical and Computer Eng., Northwestern University, Evanston, IL 60208, USA
Email: †kramnik@berkeley.edu, ‡vlada@berkeley.edu

ESSCIRC 2022 - IEEE 48th European Solid State Circuits Conference (ESSCIRC) | 978-1-6654-8494-7/22/$31.00 ©2022 IEEE | DOI: 10.1109/ESSCIRC55480.2022.9911513

***Abstract*—Integrated photonics provides scalability needed for useful photonic quantum information processing. Many optical resonators must be aligned to the same pump wavelength to produce sources of quantum-correlated photon pairs that drive such systems, but existing solutions rely on manual alignment or offline tuning based on external photodiodes and bulky off-chip electronics, limiting scalability. Here we demonstrate feedback control of four-wave mixing (stimulated and spontaneous) in a silicon microring using circuits integrated alongside photonics in a standard 45 nm CMOS foundry process. The carrier-sweepout-generated feedback signal enables *in-situ* operation in the photon-pair generation regime, which is a key building block enabling large-scale CMOS quantum-photonic systems-on-chip.**

I. Introduction

Integrated silicon photonics is an appealing quantum photonics technology platform due to its compatibility with scalable, high-fidelity CMOS manufacturing and its ability to operate at standard telecommunication wavelengths [1], [2]. Sources of indistinguishable quantum-correlated photon pairs produced by spontaneous four-wave mixing (FWM) in microring resonators are a basic building block required in many implementations of systems for quantum networking and information processing [2]. A key challenge in scaling these systems is maintaining a lock between the narrow-linewidth resonance of the microring cavity and the pump laser [3]. With higher pump powers required to maximize pair count rates, silicon microrings exhibit thermal bistability caused by self-heating from absorbed pump power [4] and can exhibit free-carrier oscillations as thermal and free-carrier dispersions take turns pushing the resonance wavelength in opposite directions [5]. These effects are substantially exacerbated by the high Q-factors needed for efficient four-wave mixing (FWM), around $10\times$ greater than those found in microring-based silicon-photonic data links [4]. Here we demonstrate the first feedback-controlled microring resonator system, with circuits implemented alongside photonics in a 45 nm SOI CMOS process, that resolves both of these issues and operates continuously during stimulated and spontaneous (photon-pair generation) four-wave mixing experiments. To our knowledge, this is the highest-Q microring wavelength-locked via an integrated thermal tuning control loop to date.

This work was funded in part by NSF EQuIP program grant #1,842,692, Packard Fellowship #2012-38222, and the Catalyst Foundation.

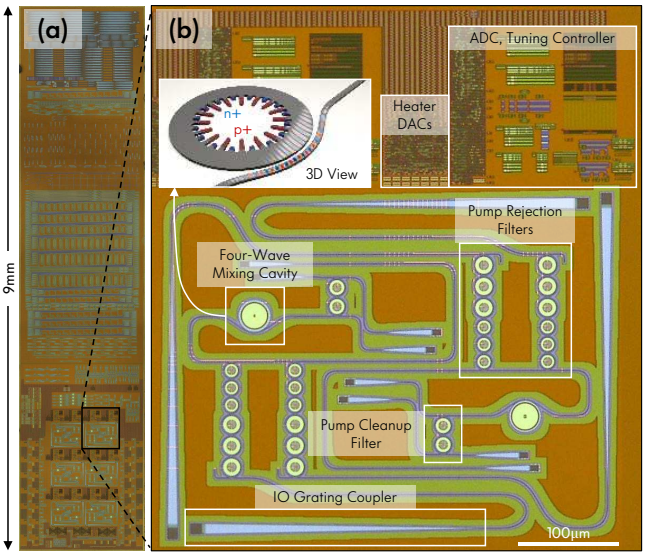

Fig. 1. (a) Die micrograph after XeF_2 etch to enable photonics, (b) two interleaved quantum-correlated photon-pair generator system sites with 3D render of carrier-sweepout, FWM-optimized microring structure (inset).

II. CMOS Quantum Photonics

A. Monolithic Electronic-Photonic CMOS Process

A 2×9 mm electronic-photonic test chip with quantum photonics and integrated circuits, shown in Fig. 1(a), was fabricated in GlobalFoundries' 45RFSOI CMOS process. Twelve pairwise interleaved quantum-correlated photon-pair generator systems occupy the bottom part of the chip, with each pair consuming 0.34 mm^2 ($550\,\mu\text{m} \times 620\,\mu\text{m}$) area including control circuits. The die is flip-chip packaged onto an FR-4 PCB for electrical interfacing and the Si substrate is removed using XeF_2 etch to enable photonics and allow optical access from the exposed back side of the chip. Optical waveguides, microring resonators and filters, and grating couplers are patterned in the transistor silicon layers to create photonic circuits alongside electronics, as shown in Fig. 1(b). We previously demonstrated passive quantum photonics in this process, including on-chip pump-rejection filters, and a manually-tuned (open-loop) photon-pair source [6], [7]. In this work, similar on-chip pump cleanup and pump rejection filters are bypassed and only the photon-pair source ring is active.

B. Microring-Based Photon-Pair Source

Four-wave mixing occurs in silicon due to its $\chi^{(3)}$ optical nonlinearity. A microring cavity resonantly enhances this effect, increasing the production rate of spontaneously-generated photon-pairs used for quantum information processing. Our system is built around a silicon microring cavity with optimized width and radius to trade off mode volume, bend loss, and integrated dispersion for optimal pair generation rate within the constraints of the CMOS platform. It contains interleaved p-i-n diode regions for carrier sweepout with geometry tailored to reduce free-carrier absorption in the area containing the optical mode, resulting in an intrinsic Q of 100,000 and loaded Q of 41,200 (FWHM $= f_o/Q = 4.7\,\text{GHz}$) when coupled to the bus waveguide, measured at $\lambda = 1552\,\text{nm}$. These all-silicon devices exhibit responsivity of 1–3 mA/W from defect-state absorption (depending on doping geometry) at $-10\,\text{dBm}$ on-chip illumination in C-band, requiring high-sensitivity readout electronics to detect the weak photocurrent signal on the order of hundreds of nA at typical pump powers ($-10\,\text{dBm}$ to $0\,\text{dBm}$, the high end being limited by multi-pair production). Unlike microrings used for classical optical datacom, the resonant frequency of a cavity used for four-wave mixing must be aligned precisely with the laser wavelength in order to optimize the pair generation rate, which falls off sharply with the detuning. This necessitates precise thermal tuning control that balances on the edge of instability to capture as much pump power in the resonator as possible.

C. On-Chip Tuning Circuits

Fig. 2 shows a schematic of the integrated feedback control circuits, adapted from the design previously used for readout of photonic ultrasound and bio-sensors [8]. The microring's photocurrent is fed into an analog frontend consisting of programmable-gain inverter-based transimpedance amplifiers (TIAs) and offset-adjustment current DACs. A pseudo-differential scheme with a sense arm and replica reference arm is adopted in order to improve CMRR and reject power supply noise coupled from the digital sections. The amplified photocurrent is then digitized by a 9-bit differential SAR ADC, accumulated 512 times on-chip for averaging, and sent to a digital controller and scan chain interface to an external FPGA. A sigma-delta DAC (10-bit pulse density modulator) drives a disk-shaped heater in the center of the source ring, which has increased thermal capacitance to improve filtering of the noise-shaped spectrum, and can be set either by the on-chip digital controller or scan chain, enabling closed-loop control of the microring's resonance frequency via thermal tuning. A switching DAC is used here to increase efficiency and avoid overheating and degradation of the output transistor. The overall wavelength tuning range is approximately 1 nm (depending on HVDD), resulting in an LSB step of 980 fm (122 MHz), which is fine enough to tune within 99% of the Lorentzian peak given the linewidth of the loaded resonator. Self-heating of the microring from absorbed pump laser power pushes its resonance point to longer wavelengths as the heater

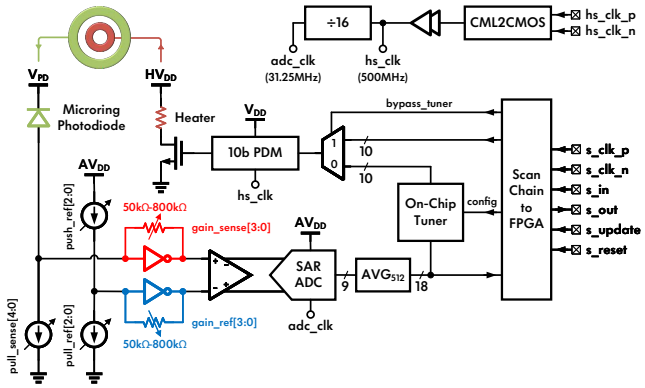

Fig. 2. Schematic diagram of readout and tuning controller circuits integrated alongside each four-wave mixing microring cavity.

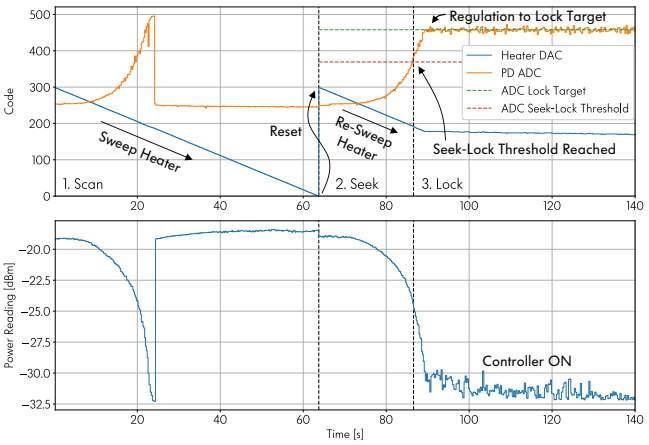

Fig. 3. Photon-pair source feedback controller waveforms and state transitions (top) and external through port monitor power (bottom), which is not used for feedback control. The slight downward slope in the through-port power is likely due to drift in the alignment of input and output coupling fibers.

is swept from hot to cold, further improving the effective resolution as the pump power is increased.

For each setting of the pump laser power and transimpedance gain ($800\,\text{k}\Omega$ in the experiments reported here) the analog frontend is automatically calibrated by sweeping the offset-calibration current DACs, which speeds up experiments by eliminating manual tuning of the circuits. The ADC readings are recorded and the current DACs are set with the goal of maximizing the photocurrent sensitivity and dynamic range. The slope of the ADC readings with respect to the sense-arm pull DAC allows the photocurrent sensitivity to be calculated since the two are summed at the input of the sense arm and it is maximized when the sense arm is biased near midrail. On the other hand, the dynamic range is maximized by introducing some offset between the sense and reference arms to pull the ADC reading as low as possible, since the photocurrent can only pull it back up, but this can also start to saturate the differential input stage and degrade the photocurrent sensitivity. In practice the two effects can be traded off by maximizing a figure-of-merit defined as the product of ADC range and photocurrent sensitivity.

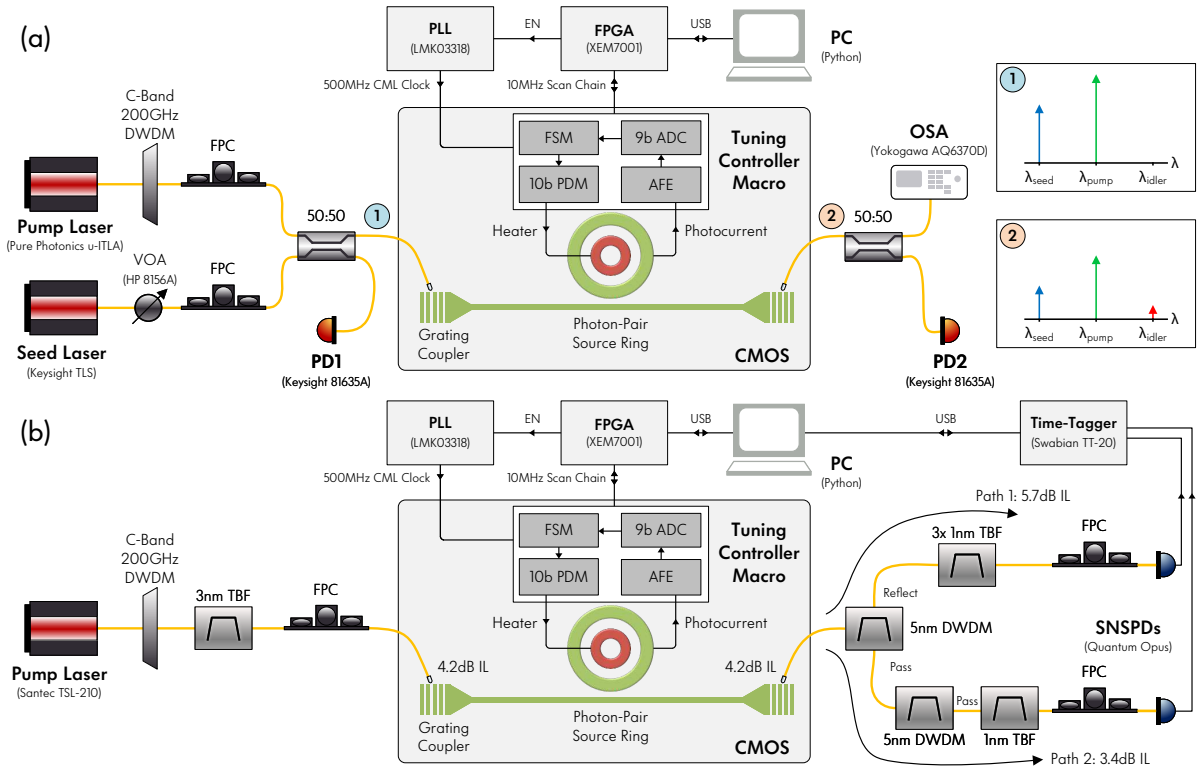

Fig. 4. (a) Stimulated four-wave mixing experimental setup and spectra, (b) spontaneous four-wave mixing experimental setup enabling simultaneous feedback control and single-photon measurements using superconducting nanowire single-photon detectors (SNSPDs).

III. Chip Measurements

A. Wavelength Locking

Fig. 3 shows waveforms from a feedback control experiment where the microring's resonant wavelength is locked to a fixed pump laser. After auto-calibration of the analog frontend, a 3-step finite state machine (FSM) engages and sweeps down the heater code to find the peak photocurrent (scan state), resets and finds the resonance again (seek state), and finally locks to a point near the maximum (lock state). The cavity must be returned to the hot state after sweeping past the laser to defeat the hysteresis created by self-heating [4]. In the lock state, a PI controller with integral deadband around the setpoint rejects noise from the analog section to eliminate spurious dithering of the heater DAC. A feedback controller is implemented within the digital logic on the chip with a different FSM optimized for locking with a fixed detuning between the laser and resonator, but we use off-chip control via scan chain interface to an FPGA and PC to implement our modified tuning algorithm and lock closer to the photocurrent peak (at 95 % peak current, presently limited by fiber stability). No Peltier cooler or other off-chip thermal stabilization is required. In this work the sample rate is limited to 4 Hz by the slow interface between the control FPGA and Python script used to prototype the control algorithm, but could be boosted up to 1 kHz by implementing the same control logic on the FPGA (which is then limited by the test chip's total scan chain length and 10 MHz scan clock).

B. Four-Wave Mixing

Using the dual-laser setup illustrated in Fig. 4(a) we measure -41.2 dB conversion efficiency at -5.8 dBm on-chip pump power in the stimulated FWM regime — Fig. 5(a,b). This is comparable to manually-aligned passive microrings in this process [9], indicating that the addition of dopings for carrier sweepout does not compromise performance (stimulated FWM efficiency is not affected by insertion losses after the resonator, making it a more reliable way to compare different resonators than off-chip photon-pair count rates). The pump laser in this case was a commercial micro-ITLA (integrated tunable laser) module, enabling future miniaturization of the system into a test-equipment-free complete module.

We also characterized quantum-correlated photon-pair generation under feedback control using the setup illustrated in Fig. 4(b). We recorded up to 300 ccps (coincidence counts per second) off-chip pair generation rate and a maximum coincidences-to-accidentals ratio (CAR) of 38 with -1.6 dBm and -5.6 dBm on-chip pump powers respectively, using 60% quantum efficiency in C-band superconducting nanowire single photon detectors (SNSPDs) — Fig. 5(c,d). Grating coupler insertion losses (4.2 dB per coupler) and external pump-rejection filter insertion losses (3.4 dB and 5.7 dB per channel) also limited the measured count rates. Since losing a photon in either channel of the experiment results in a missed coincidence count, the sum of insertion losses in both channels (21.9 dB) can be used to estimate the on-chip count rate, yielding a max-

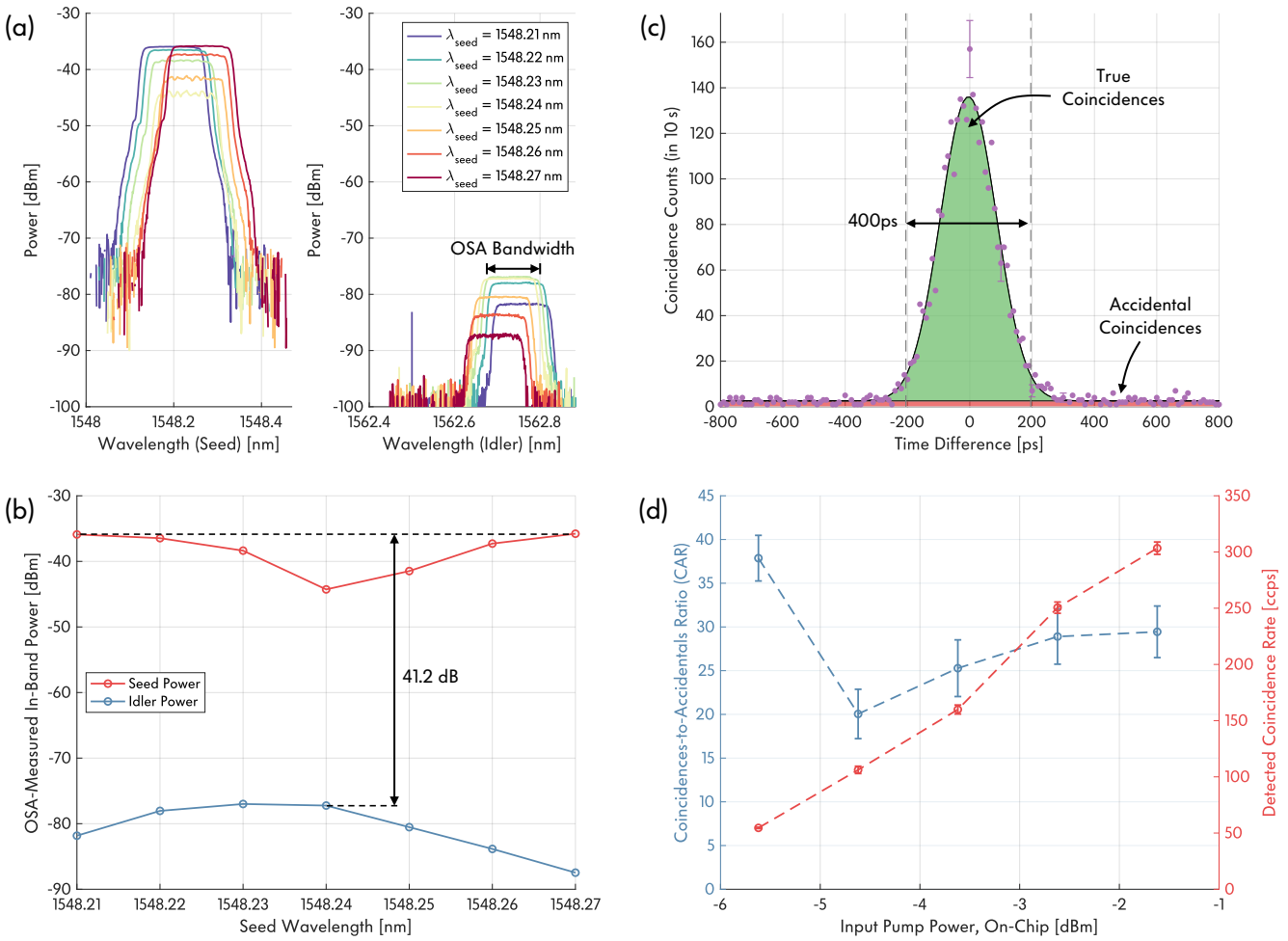

Fig. 5. Stimulated FWM through port spectra (a) and seed and idler powers and conversion efficiency (b), with -5.8 dBm on-chip pump power. Spontaneous FWM coincidence histogram with -1.6 dBm on-chip pump power (c) and CAR and coincidence count rate with active feedback control vs. pump power (d).

imum on-chip pair rate of 46.5 kccps. In separate experiments we have wavelength-aligned the low-loss integrated pump-rejection filters using on-chip circuits [10], paving the way for a fully-monolithic photon-pair generator system.

IV. Conclusion

In this work we demonstrate feedback control of a silicon four-wave mixing cavity with electronics and photonics fabricated together on the same die in a 45 nm CMOS foundry process. This represents a new step towards creating a self-contained source of entangled photons that incorporates active photonic devices and feedback control circuits onto the same CMOS chip. We utilize a standard 45 nm foundry process that can support hundreds of electronically-controlled photonic devices operating alongside millions of transistors, used previously for classical information processing [11].

Acknowledgment

We thank the Berkeley Wireless Research Center and Berkeley Emerging Technologies Center for support and Ayar Labs for chip fabrication.

References

[1] Rudolph, T. "Why I am optimistic about the silicon-photonic route to quantum computing", APL Photonics. 2, 030901 (2017).
[2] Silverstone, J.W. *et al.*, "Silicon Quantum Photonics", IEEE J. Sel. Top. Quantum Electronics 22, 390-402 (2016).
[3] Carolan, J. *et al.*, "Scalable feedback control of single photon sources for photonic quantum technologies", Optica 6, 335-340 (2019).
[4] Sun, C. *et al.*, "A 45nm CMOS-SOI Monolithic Photonics Platform With Bit-Statistics-Based Resonant Microring...", IEEE JSSC (2016).
[5] Johnson, T. J. *et al.*, "Self-induced optical modulation of the transmission through a high-Q silicon microdisk resonator", Opt. Express (2006).
[6] Gentry, C. M. *et al.*, "Monolithic Source of Entangled Photons with Integrated Pump Rejection", CLEO (2018).
[7] J. Fargas-Cabanillas, D. Kramnik, A. Ramesh, *et al.*, "Tunable Source of Quantum-Correlated Photons with Integrated Pump...", FiO (2021).
[8] C. Adamopoulos, P. Zarkos, *et al.*, "Lab-on-Chip for Everyone: Introducing an Electronic-Photonic Platform...", IEEE OJ-SSCS (2021).
[9] Gentry, C. M. *et al.*, "Quantum-correlated photon pairs generated in a commercial 45nm...", Optica 2, 1065-1071 (2015).
[10] Fargas Cabanillas, J. M. *et al.*, "Monolithically Integrated High-Order Vernier Filters for Electronic-Photonic...", CLEO (2022).
[11] C. Sun, M.T. Wade, Y. Lee, *et al.* "Single-chip microprocessor that communicates directly using light", Nature 528, 534–538 (2015).